The Brownian Ratchet and Power Stroke Models for Posttranslational Protein Translocation into the Endoplasmic Reticulum

Timothy C. Elston

Biomathematics Graduate Program/Department of Statistics, North Carolina State University, Raleigh, North Carolina 27695-8203 USA

ABSTRACT   A quantitative analysis of experimental data for posttranslational translocation into the endoplasmic reticulum is performed. This analysis reveals that translocation involves a single rate-limiting step, which is postulated to be the release of the signal sequence from the translocation channel. Next, the Brownian ratchet and power stroke models of translocation are compared against the data. The data sets are simultaneously fit using a least-squares criterion, and both models are found to accurately reproduce the experimental results. A likelihood-ratio test reveals that the optimal fit of the Brownian ratchet model, which contains one fewer free parameter, does not differ significantly from that of the power stroke model. Therefore, the data considered here cannot be used to reject this import mechanism. The models are further analyzed using the estimated parameters to make experimentally testable predictions.

INTRODUCTION

Many proteins synthesized in the cytosol must be transported across the membrane of the endoplasmic reticulum (ER). Translocation proceeds through a protein-conducting channel (Simon and Blobel, 1991) and can occur either co-translationally, with the ribosome attached directly to the import channel, or post-translationally, after the nascent protein has been released from the ribosome. In this manuscript I focus exclusively on the latter mechanism. In a previous article (Elston, 2000b) I developed a mathematical formulation for two models of post-translational translocation: the Brownian ratchet model and the power stroke model. Here I test the validity of both models by fitting them to experimental data. This analysis reveals that translocation involves a single rate-limiting step. I show that if this slow step is attributed to release of the signal sequence from the channel, then both models accurately reproduce the experimental results. Even though the power stroke model contains an additional free parameter, a likelihood-ratio test reveals that it does not produce a significantly better fit than the Brownian ratchet model.

In all the experiments considered in this manuscript, prepro-α-factor is the translocation substrate. A signal sequence located at the amino-terminus of prepro-α-factor targets it for translocation. The signal sequence is inserted into the channel as a loop with a small portion exposed to the ER lumen (Plath et al., 1998). The channel-forming protein is Sec61p (Gorlich and Rapoport, 1993), which is one component of the membrane-bound Sec complex (Deshaies et al., 1991; Panzer et al., 1995). On the lumenal side of the channel Sec61p associates with a Sec-62/63p com-

plex. Translocation requires the presence of lumenal BiP (Vogel et al., 1990). BiP is a member of the Hsp-70 family of ATPases and interacts with both prepro-α-factor and the J-domain of Sec63p (Brodsky and Schekman, 1993; Lyman and Schekman, 1995; Matlack et al., 1997, 1999; Sanders et al., 1992). The interaction between BiP and the J-domain stimulates the ATPase activity of BiP (Corsi and Schekman, 1997) and allows BiP to trap a wide range of peptides (Misselwitz et al., 1998). While BiP is required to provide directionality to the translocation process, its functional role has not been determined. Two possible mechanisms for BiP have been suggested. In the Brownian ratchet model (BRM), BiP acts passively to prevent backsliding of the translocation substrate through the channel (Schneider et al., 1994; Simon et al., 1992). Whereas, in the power stroke model (PSM), BiP undergoes a conformational change that generates a power stroke that pulls the translocation substrate through the channel (Glick, 1995).

I begin with a detailed description of both models and their underlying mathematical assumptions. The models are then fit to experimental data using a least-squares criterion. To perform a global fit to the data requires the use of simplified versions of both models. The assumptions that underlie these simplifications are verified by directly comparing the simpler models' behavior with Monte Carlo simulations of the full processes. The parametrized models are then mathematically characterized and used to make experimentally testable predictions.

MODEL DESCRIPTIONS AND ASSUMPTIONS

This section provides a description of both models. I assume that when prepro-α-factor associates with the channel, it forms a loop with a small portion of the polypeptide exposed to the lumen (Plath et al., 1998) (see Fig. 1). The interaction free energy between the signal sequence and the channel, ΔG, is spread equally over the length of the signal sequence. All other interactions between the channel and
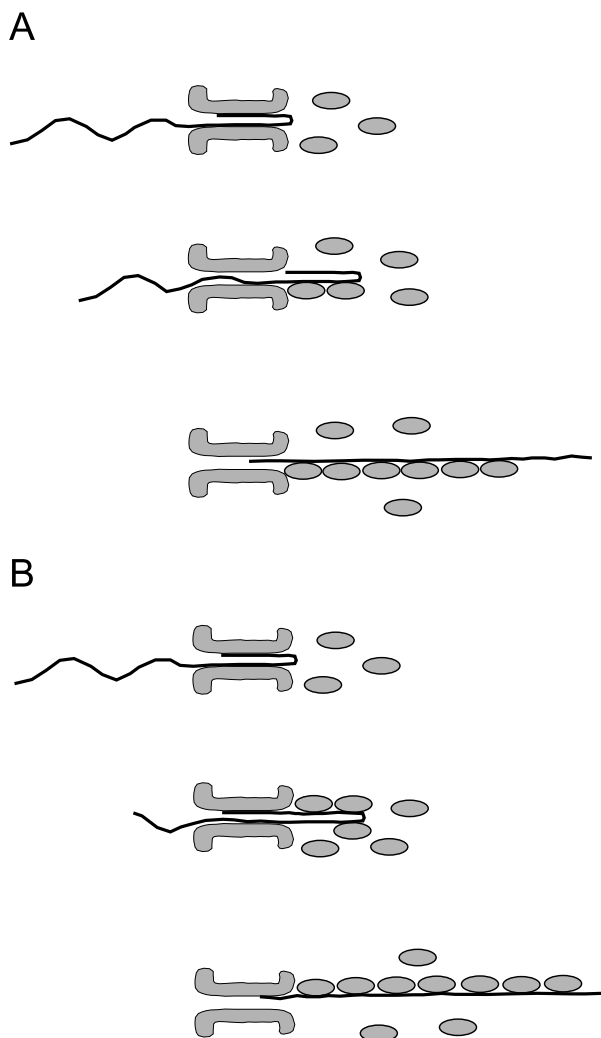
A

B

FIGURE 1   Two scenarios for the translocation process. (*A*) A prepro-α-factor protein is initially inserted into the channel as a loop. Within the lumen of the ER the translocation substrate interacts with BiP molecules, shown as elliptical particles in the figure. The loop moves as a unit out of the channel at the start of translocation. The loop is assumed to be two BiP binding sites in length, roughly the length of the signal sequence. (*B*) Again, the protein is inserted into the channel as a loop. However, in this case the signal sequence remains in the channel until after the rest of the polypeptide has been translocated. In both scenarios the strong interaction between the signal sequence and the channel makes translocation of the signal sequence the rate-limiting step in the process.
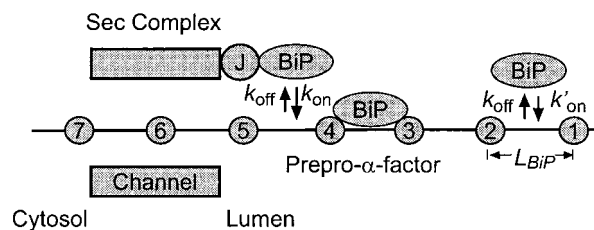

FIGURE 2   A model diagram with specific BiP binding sites. The numbered circles on the prepro-α-factor protein indicate the ratchet sites where the rear edge of a BiP molecule binds. The sites are evenly spaced with a distance L_{BiP} between each site. When a ratchet site is within a distance L_{BiP} of the channel, the J-activated association rate is k_{on} [BiP], otherwise it is k'_{on}[BiP]. The dissociation rate is k_{off} for all sites. For the PSM, when an occupied site is within a distance L_{BiP} of the channel, the BiP molecule generates a constant power stroke of strength F_{ps}.

prepro-α-factor are modeled using an effective diffusion coefficient D (Elston, 2000a, b; Lubensky and Nelson 1999; Muthukumar, 1999, 2001). I consider two translocation scenarios. In case A, the loop moves as a unit and the signal sequence leaves the channel at the start of translocation, whereas in B the signal sequence remains in the channel until the rest of the polypeptide has been translocated. In both scenarios the free energy associated with straightening the polypeptide is ignored. This is not unreasonable, because prepro-α-factor does not posses any tightly folded

domains, and the free energy required to unfold a loosely folded protein is small (Chauwin et al., 1998; Park and Sung, 1996).

Translocation requires that lumenal BiP molecules, which are shown as elliptical particles in Fig. 1, bind to the prepro-α-factor protein. Two different scenarios for BiP binding are considered. In the first case, I postulate the existence of specific BiP binding sites along prepro-α-factor (specific binding). In the second scenario, a BiP molecule can bind as soon as there is sufficient distance between the channel and the back edge of the nearest bound BiP molecule (nonspecific binding). Fig. 2 is a schematic diagram of the system for the specific binding case. The binding sites are assumed to be evenly spaced along the translocation substrate. The maximum number of BiP molecules that can bind to prepro-α-factor is an adjustable parameter denoted by N. When a BiP molecule binds to prepro-α-factor, its trailing edge is located at one of the circles drawn on the polypeptide. That is, these points indicate the ratchet sites. Prepro-α-factor consists of 165 amino acids, which corresponds to a length of 58 nm (0.35 nm per amino acid). Therefore, the distance between ratchet sites is $L_{BiP} = 58/N$ nm. All the sites within the lumen are accessible to BiP binding. I assume that a BiP molecule trapped by the J-domain of Sec63p can associate with the binding site while the back edge of the site is within a distance L_{BiP} of the channel. This effective trapping distance has been chosen for mathematical simplicity. However, it can be significantly shortened without affecting the results. When an empty site is within the trapping distance the J-activated association rate is k_{on}[BiP], where the brackets indicate concentration. For empty sites further within the lumen, the association rate is k'_{on}[BiP] $< k_{on}$[BiP]. For all the binding sites the dissociation rate is k_{off}. For the PSM, when the binding site nearest the channel is occupied, the BiP molecule is assumed to be bound to both the J-domain and the translocation substrate. It then undergoes a conformational change that generates a constant force F_{ps} over the entire

TABLE 1 Estimated model parameters

Symbol	Meaning	Value	
		First out	Last out
BRM			
N	Maximum number of BiP molecules	10	10
k_{off}	BiP dissociation rate	0.0277 s^{-1}	0.0297 s^{-1}
k_{on}	J-activated BiP association rate	351.2 s^{-1} μM^{-1}	337.7 s^{-1} μM^{-1}
ΔG	Signal sequence binding free energy	73.7 pN-nm	79.7 pN-nm
		(44.4 kJ/mol)	(48.0 kJ/mol)
D	Diffusion coefficient	160.0 nm^2/s	415.1 nm^2/s
k'_{on}	BiP association rate	0.00045 s^{-1} μM^{-1}	0.00048 s^{-1} μM^{-1}
PSM			
N	Maximum number of BiP molecules	10	10
k_{off}	BiP dissociation rate	0.0262 s^{-1}	0.0271 s^{-1}
k_{on}	J-activated BiP association rate	310.3 s^{-1} μM^{-1}	294.2 s^{-1} μM^{-1}
ΔG	Signal sequence binding free energy	79.8 pN-nm	83.1 pN-nm
		(48.0 kJ/mol)	(50.0 kJ/mol)
D	Diffusion coefficient	192.9 nm^2/s	320.1 nm^2/s
k'_{on}	BiP association rate	0.00040 s^{-1} μM^{-1}	0.00041 s^{-1} μM^{-1}
F_{ps}	Power stroke	1.63 pN	3.81 pN

The estimated model parameters for the BRM and PSM found from a global fit to the data. The column First Out contains parameter values for the scenario in which the signal sequence leaves the channel first, and the column Last Out is for the case in which the signal sequence leaves last.

trapping distance L_{BiP}, which pulls the polypeptide through the channel. In reality, a power stroke would not generate a constant force. However, F_{ps} should be interpreted as the average power stroke over L_{BiP} (Elston, 2000b). Note that for the PSM, prepro-α-factor is still ratcheted by BiP. That is, the BRM represents a limiting case of the PSM in which $F_{ps} \rightarrow 0$. As is shown below, one advantage of assuming specific binding sites is that approximate methods can be used to estimate the model parameters.

For nonspecific binding, all that is required for a trapped BiP molecule to associate with the translocation substrate is that a distance of at least L_{BiP} exist between the channel and the nearest bound BiP molecule. The rest of the assumptions for nonspecific binding are identical to the specific binding case.

PARAMETER ESTIMATION

In this section I estimate the model parameters by fitting experimental data. Monte Carlo simulations are too computationally expensive to be used effectively for fitting the data. Therefore, approximate methods are developed. The validity of this approach is verified in the next section, where the results of full Monte Carlo simulations using the estimated parameter values are presented. Table 1 is a summary of the estimated parameter values for both models.

The analysis focuses on data taken using the experimental procedure developed by Matlack et al. (1997). In these experiments radiolabeled prepro-α-factor is mixed with proteoliposomes containing the channel complex in the absence of BiP or ATP. The signal sequence targets prepro-α-factor for translocation. The signal sequence binds tightly to the channel and in the absence of BiP, prepro-α-factor is effec-

tively stalled in the channel. The membrane is then removed using a detergent, and the reaction is started by adding BiP and ATP. Finally, immunoprecipitation against the channel complex is performed. Figs. 3 and 6 show the types of data that are generated using this procedure (Matlack et al., 1999). In Fig. 3 A two data sets are shown. The ×'s are the fraction of prepro-α-factor molecules released from the Sec complex as a function of time at 1 μM BiP, and the +'s are the fraction of prepro-α-factor molecules released and free of BiP as a function of time. In Fig. 6, the ×'s are the fraction of prepro-α-factor molecules remaining bound to the channel after 10 min as a function of BiP concentration.

Model-independent parameters

First I determine what information can be found from the data without assuming a specific model of translocation. I start with the fraction released data (*FR*). In Fig. 3 B 1-FR has been graphed on a semi-log plot. Only the first four data points are shown, because the remaining three are essentially equal to one. Plotted this way, the data appear linear. This means the fraction released as a function of time can be written as

$$FR(t) = 1 - \exp(-k_{out}t) \qquad (1)$$

Using a least-squares criterion to fit the fraction released data, we find $k_{out} = 0.0071$ s^{-1} = 0.43 min^{-1}. The solid curves shown in Fig. 3 A and B are the fit to the data. The exponential nature of the data indicates translocation involves a single rate-limiting step. To clarify this point and develop the idea of a first passage time, I illustrate the relationship between $FR(t)$ and the time required for release
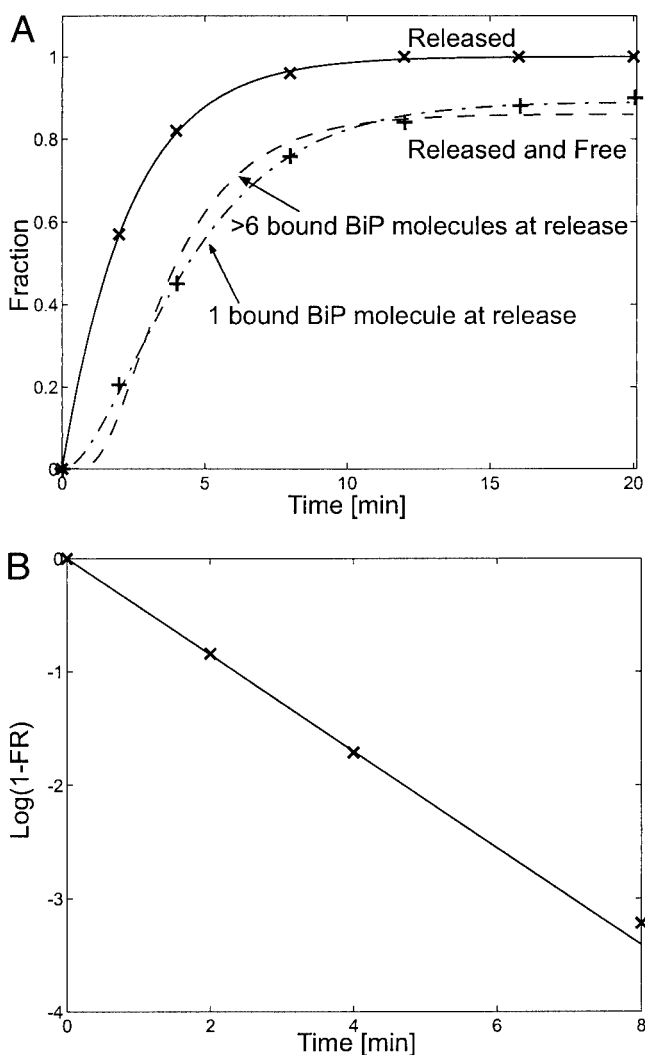
FIGURE 3 (A) The ×'s are data points for the fraction of prepro-α-factor molecules that have been released from the channel as a function of time at 1 μM BiP. The solid curve is the expression FR = 1 − exp($-k_{out}t$) with k_{out} = 0.0071 s^{-1}. The +'s are data points for the fraction of prepro-α-factor molecules not only released from the channel, but also free of BiP molecules. The dot-dashed curve is a fit to the data assuming that at the time of release the translocation substrate has one bound BiP molecule. The dashed curve assumes that at the time of release the translocation substrate has at least seven bound BiP molecules. All the experimental data are from Matlack et al. (1999). (B) A semi-log plot of 1-FR showing the exponential nature of the fraction-released data. The solid line has a slope of k_{out}.

from the channel, T. T is a random variable, whose probability density can be determined from $FR(t)$ using the following reasoning. The probability that release occurs between t_1 and a later time t_2 is given by

$$\Pr[t_1 \leq T \leq t_2] = FR(t_2) - FR(t_1) = \int_{t_1}^{t_2} f(t)dt \quad (2)$$

where the last equality holds from the definition of the

probability density $f(t)$ for T. The above expression implies that

$$f(t) = \frac{dFR}{dt} = k_{out} \exp(-k_{out}t), \quad (3)$$

which can be verified by direct substitution of Eq. 3 into Eq. 2. Therefore, T is exponentially distributed and characterized solely by the rate k_{out}. The mean first passage time is $E[T] = 1/k_{out} = 2.3$ min.

Note that the exponential distribution takes on its maximum value at $t = 0$. Therefore, the exponential nature of the data is only approximately true, because translocation requires a finite amount of time. It is possible that the fraction of prepro-α-factor released does show a lag at early times, where data are not available. To test this possibility I refit the data assuming a two-step process. In this case, $FR(t)$ has the form

$$FR(t) = 1 - \frac{k_2e^{-k_{out}t} - k_{out}e^{-k_2t}}{k_2 - k_{out}} \quad (4)$$

where the rate k_2 is an extra free parameter. The additional parameter only very slightly improved the fit, and the best fit occurred when the two rates differed by over two orders of magnitude. When rates that differed by less than an order of magnitude were used, the fit was significantly worse; thus, justifying the assumption of a single rate-limiting step. I show below that the rate-limiting step can be attributed to the release of the signal sequence from the channel.

Next consider the fraction released and free data (Fig. 3 A). The first thing to note is that these data do not asymptote to 1. I assume that this effect is a result of BiP binding to prepro-α-factor without J-activation, which continues to occur after prepro-α-factor has been released from the channel. However, it is also possible that this effect is attributable to unspecific co-immunoprecipitation (Liebermeister et al., 2001). The fraction released and free data are not well fit by a single exponential (not shown). It was shown above that prepro-α-factor is released from the channel at an exponential rate k_{out}. The number of BiP molecules bound to a prepro-α-factor molecule at the time of release is a random variable. However, for simplicity I assume that for the case in which the signal sequence leaves first, a prepro-α-factor molecule has $N - 3$ binding sites occupied at the time of release. The rationale for three empty sites is that the signal sequence is two sites long (see Fig. 1) and once the last binding site has entered the lumen, the translocation substrate rapidly diffuses away from the channel, not allowing enough time for a BiP to bind to the last site. I have investigated the effects of letting the number of occupied sites at the time of release vary between N and $N - 3$, but for cases in which $N > 9$ the results are virtually unchanged. Once the prepro-α-factor protein is free of the channel, BiP dissociates from it with a rate k_{off} and associates with rate k'_{on} [BiP]. Note that if BiP molecules bind independently to

prepro-α-factor, then the equilibrium probability of an empty chain p_0^{eq} is

$$p_0^{\text{eq}} = \left(\frac{k_{\text{off}}}{k_{\text{off}} + k'_{\text{on}}[\text{BiP}]}\right)^N \qquad (5)$$

This value represents the asymptotic value of the fraction released and free data reached after long times.

Let the random variable $M(t)$ denote the number of BiP molecules bound to a released prepro-α-factor protein at time t. The probabilities $p_i(t) = \Pr[M(t) = i]$ satisfy Eqs. 17–21 of Appendix A. These equations are solved numerically and $p_0(t)$ is fit to the data by adjusting the parameters N, k_{off} and k'_{on}. The results are shown in Fig. 3 A, where again a least-squares criterion has been used. The data were fit with values of N ranging from 4 to 10. Surprisingly, the best fit, shown as the dot-dashed line in Fig. 3 A, occurred when $N = 4$, in which case there is only 1 BiP molecule bound at the time of release. The values of the other two parameters are $k_{\text{off}} = 0.0066$ s^{-1} and $k'_{\text{on}} = 0.00019$ μM^{-1} s^{-1}. Using these values, $p_0^{\text{eq}} = 0.89$ and the dissociation constant $K_{\text{d}} = k_{\text{off}}/k'_{\text{on}} = 34.7$ μM. It is has been observed that at 1 μM BiP, prepro-α-factor is released from the channel with at least six or seven BiP molecules bound to it (Matlack et al., 1999). This apparent contradiction with the results from curve-fitting could be explained if one binding site on prepro-α-factor has a much stronger affinity for BiP then the others. In this case there are two rate-limiting steps in this process: release from the channel and dissociation of the tightly bound BiP molecule. To minimize the number of free parameters in the models I assume that the dissociation constants for all the sites are equal, in which case to have a significant probability of 7 BiP molecules bound at release, N must be ≥ 10. For $N \geq 10$, the fits to the data are virtually identical with higher values producing only slightly worse fits. The dashed line in Fig. 3 A represents these cases. When all the data are considered, the parameter values found when $N = 10$ produce the best fit for both models. In this case, $k_{\text{off}} = 0.024$ s^{-1} and $k'_{\text{on}} = 0.00036$ μM^{-1} s^{-1}. With these values, $L_{\text{BiP}} \approx 6$ nm, $p_0^{\text{eq}} = 0.86$, and $K_{\text{d}} = 65.8$ μM. This value of K_{d} compares well with the experimentally measured values of $K_{\text{d}} = 20$ μM at saturating ADP conditions and $K_{\text{d}} = 200$ μM at saturating ATP conditions determined by Misselwitz et al. (1998). The estimated values of N, k_{off}, and k'_{on} are used as initial guesses in the global fit performed next.

Model-dependent parameters

In the absence of BiP, 2% or less of the prepro-α-factor molecules are released from the channel after 60 min (Liebermeister et al., 2001). That is, $FR(60 \text{ min}) \leq 0.02$. Assuming the number is actually 2% implies that the average time for release from the channel is $E[T_{\text{nBiP}}] = 49$ h. If prepro-α-factor release only requires diffusion through the channel, then this time is equal to $L_p^2/(2D)$, where $L_p = 58$ nm is the length of a prepro-α-factor protein. In the presence

of BiP, the average time for release from the channel is $E[T] = 2.3$ min. Therefore, the stimulation caused by BiP is $E[T_{\text{nBiP}}]/E[T] \approx 1000$. Under optimal conditions $E[T] = L_p/\nu_{\text{max}}$, where ν_{max} is the maximum possible velocity of the translocation substrate and depends on the model. This leads to the relationship

$$\frac{E[T_{\text{nBiP}}]}{E[T]} = \frac{L_p \nu_{\text{max}}}{2D} \qquad (6)$$

For the BRM, $\nu_{\text{max}} = 2D/L_{\text{BiP}}$ and for a large power stroke, $\nu_{\text{max}} \approx DF_{\text{ps}}/k_{\text{B}}T$, where $k_{\text{B}}T = 4.1$ pN-nm is the Boltzmann constant times the absolute temperature. When these expressions for ν_{max} are used in Eq. 6, we find $L_{\text{BiP}} = 0.06$ nm for the BRM and $F_{\text{ps}} = 141$ pN for the PSM. Both these values are physically unrealistic. Therefore, the assumption that escape from the channel only requires diffusion is incorrect.

The amount of stimulation caused by BiP can be greatly increased if the signal sequence binds tightly to the channel. The assumed free energy landscapes for the prepro-α-factor-channel complex are shown in Fig. 4 A. The binding energy of the signal sequence with the channel is ΔG. This interaction might arise from hydrophobic or electrostatic interactions and prohibits the signal sequence from moving backward or forward. In the absence of BiP and ATP, it is much more likely that escape occurs by prepro-α-factor backing out of the channel, because in the forward direction prepro-α-factor must still diffuse through its full length to be free of the channel. Under these conditions and if ΔG is large compared with $k_{\text{B}}T$, the average time for release from the channel is approximately given by

$$E[T_{\text{nBiP}}] = 2\frac{(2L_{\text{BiP}})^2}{D}\left(\frac{k_{\text{B}}T}{\Delta G}\right)^2 \exp\left(\frac{\Delta G}{k_{\text{B}}T}\right) \qquad (7)$$

where it has been assumed that the free energy drop is spread equally over a distance of $2 L_{\text{BiP}}$, which corresponds roughly to the length of the signal sequence. Fig. 4 B shows the effect of adding BiP; now if prepro-α-factor moves a distance L_{BiP} into the lumen, a BiP molecule can bind and prevent backsliding. The translocation substrate can then move the rest of the way out of the free energy well, at which point another BiP molecule is free to associate with it. In the limit of very fast and irreversible BiP binding, prepro-α-factor does not have to surmount a single potential barrier of ΔG, but rather two barriers of height $\Delta G/2$. Therefore, if translocation is assumed to occur instantaneously after the signal sequence has been released from the channel, the stimulation caused by BiP is

$$\frac{E[T_{\text{nBiP}}]}{E[T]} = \frac{1}{2}\exp\left(\frac{\Delta G}{2k_{\text{B}}T}\right) \approx 1000 \qquad (8)$$

from which we find a minimal value of 62 pN-nm = 37.2 kJ/mol for ΔG. For the PSM, this number can be reduced. In addition to corresponding roughly to the length of the signal
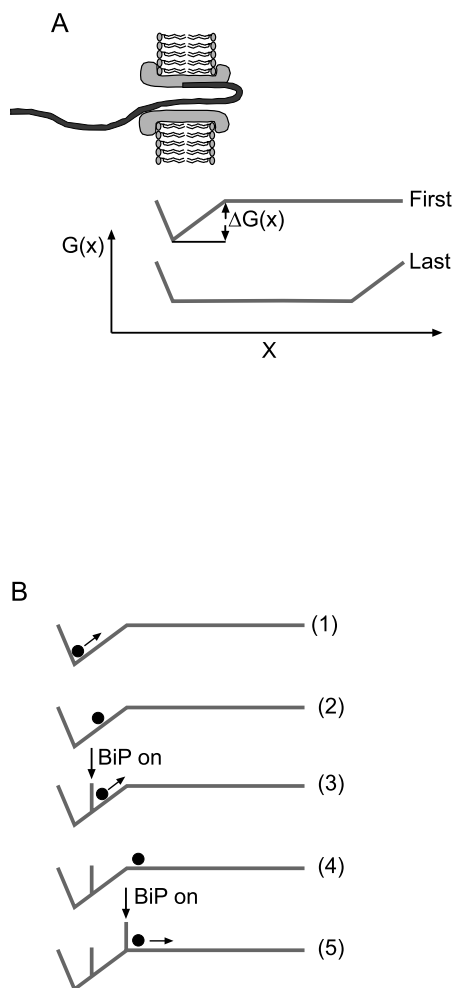
FIGURE 4 (*A*) The free energy diagrams for the interaction between prepro-α-factor and the channel. The top curve labeled First is for the scenario in which the signal sequence exists in the channel at the start of translocation, and the lower curve labeled Last is the case in which the signal sequence leaves last. The free energy well is due to strong signal sequence/channel interactions and is characterized by a depth ΔG. ΔG is distributed equally over the signal sequence. (*B*) A diagram illustrating the role of BiP in stimulating the release of the signal sequence from the channel for the signal sequence out first scenario. The particle in this diagram indicates the leading edge of a prepro-α-factor molecule. 1) The signal sequence is trapped in the channel. 2) Thermal diffusion carries the translocation substrate forward by an amount $\geq L_{\mathrm{BiP}}$. 3) A BiP molecule binds to the translocation substrate preventing backsliding. 4) Thermal diffusion carries the ratcheted prepro-α-factor out of the free energy well. In the PSM, this step is aided by a constant force F_{ps}. 5) A second BiP molecule binds, preventing backsliding into the well. Translocation then proceeds rapidly.

sequence, the rationale for distributing ΔG over two binding sites is the following. If the free energy was distributed over only one site, then at high BiP concentrations escape in the forward and backward direction would be approximately equally likely, and only a speedup of around two would be seen. If, however, the binding energy was distributed over three binding sites, then there is not a single rate-limiting

step in the process and the exponential nature of the fraction-released data is lost. It is not obvious that distributing the free energy over two binding sites leads to single rate-limiting step. However, I will show that for this case the first passage time distributions look approximately exponential. The slowest step in the process is the association of the first BiP molecule. The binding of the second BiP molecule is not as difficult, because once prepro-α-factor has moved a distance of 2 L_{BiP}, it does not experience a net force toward the channel.

I have fit the data assuming both scenarios for release of the signal sequence. In the first case, in which the signal sequence leaves the channel first, I assume that once three binding sites have passed through the channel the rest of the polypeptide moves through instantaneously. The reason for including the third site is that in this scenario there is a significant probability of the translocation substrate moving backward into the channel once two complete sites have been translocated. In the second case, in which the signal sequence leaves last, only the last two sites that make up the signal sequence are considered, because in this case once the signal sequence clears the channel the polypeptide quickly diffuses away. The validity of these approximations is verified in the next section through a comparison with Monte Carlo simulations of the full process. The model equations for the marginal density $\rho(x, t)$ for the position of prepro-α-factor are solved numerically. See Appendix A for the details of the numerical methods. The fraction remaining and $FR(t)$ are calculated from $\rho(x, t)$ as follows:

$$\text{Fraction Remaining} = \int_0^{iL_{\mathrm{BiP}}} \rho(x, t)dx = 1 - FR(t) \quad (9)$$

where $i = 3$ for the case in which the signal sequence leaves first and $i = 2$ if the signal sequence leaves last. To fit the fraction release and free data the numerically computed flux out of the channel is used in Eqs. 17–21 of Appendix A. A global fit to all three data sets using a least-squares criterion was performed. For the BRM, the estimated parameters are N, ΔG, k_{on}, k_{off}, D, and k'_{on}, and the PSM has an additional parameter F_{ps}. For every value of ΔG, the value of D is constrained to ensure that in the absence of BiP 2% or less of the prepro-α-factor molecules are released from the channel after 60 min. Table 1 lists the estimated parameter values for the two different models and two different release scenarios. We only present the results for the case in which the signal sequence leaves the channel first. The results for the case in which the signal sequence leaves last are only slightly worse. Fig. 5, *A* and *B* show the fits to fraction released and fraction released and free data for the two models. In both figures the dashed curves are the exponential fit to the fraction released data shown as the solid curve in Fig. 3 *A*. Note that the PSM better approximates the exponential nature of the data, and therefore results in
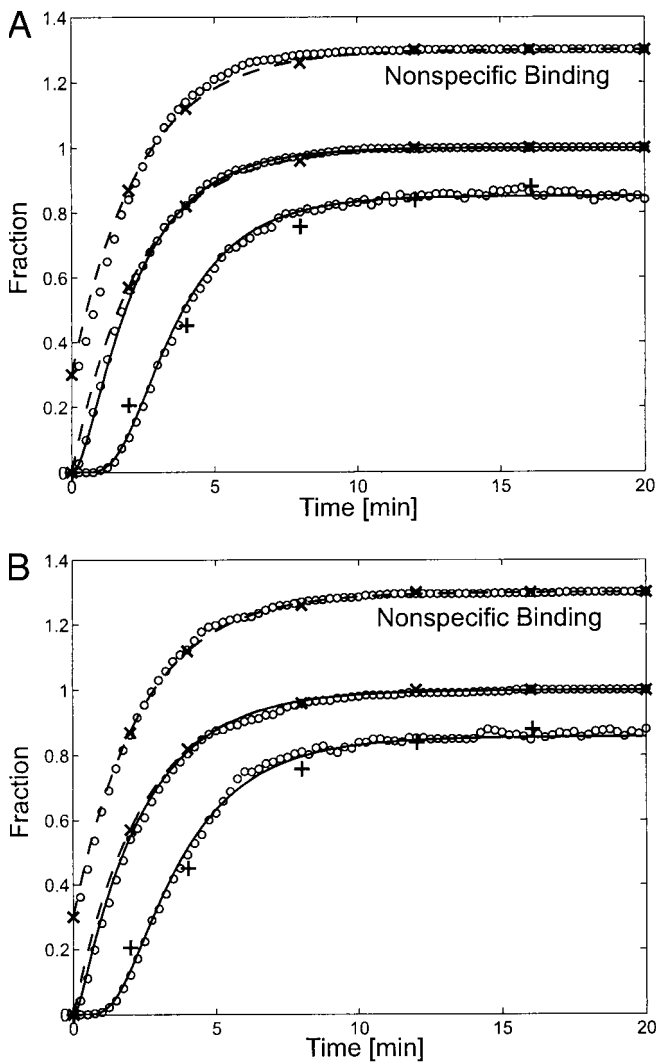
FIGURE 5 (A) Fits to the fraction released data (×) and fraction released and free data (+) for the BRM. The solid curves are the results from the simplified model described in the text in which translocation proceeds instantaneously after the third BiP binding site has moved out of the channel. The circles are the results of Monte Carlo simulations of the full process. The dashed curves are the same as the solid curve shown in Fig. 3 A, in which it is assumed that a single rate-limiting step k_{out} is involved in translocation. Also shown are the results for the fraction-released data from Monte Carlo simulations for the case of nonspecific BiP binding. These points have been offset by 0.3 for clarity. (B) The same as in A, except for the PSM. A power stroke better captures the exponential nature of the fraction-released data and provides a better overall fit.

FIGURE 6 (A) The ×'s are experimental data points for the fraction of prepro-α-factor molecules remaining bound to the channel after 10 min as a function of [BiP] (Matlack et al., 1999). The solid cure is a fit to the data using the simplified BRM. The diamonds are the results from Monte Carlo simulations for the case of nonspecific BiP binding. The error bars give 95% confidence intervals. For clarity, the results for the case of specific BiP binding are not shown. (B) The same as A, except for the PSM.

slightly better overall fit to the data. The results for the fraction remaining data are shown in Fig. 6, A and B. In all cases, there is good agreement between the experimental data and model predictions.

Fig. 7 shows the first passage time distributions for the two models. Also plotted is an exponential distribution with $E[T] = 2.3$ min. As expected, both models show nonexponential behavior at short times. However, for long times both models approximate the exponential distribution fairly
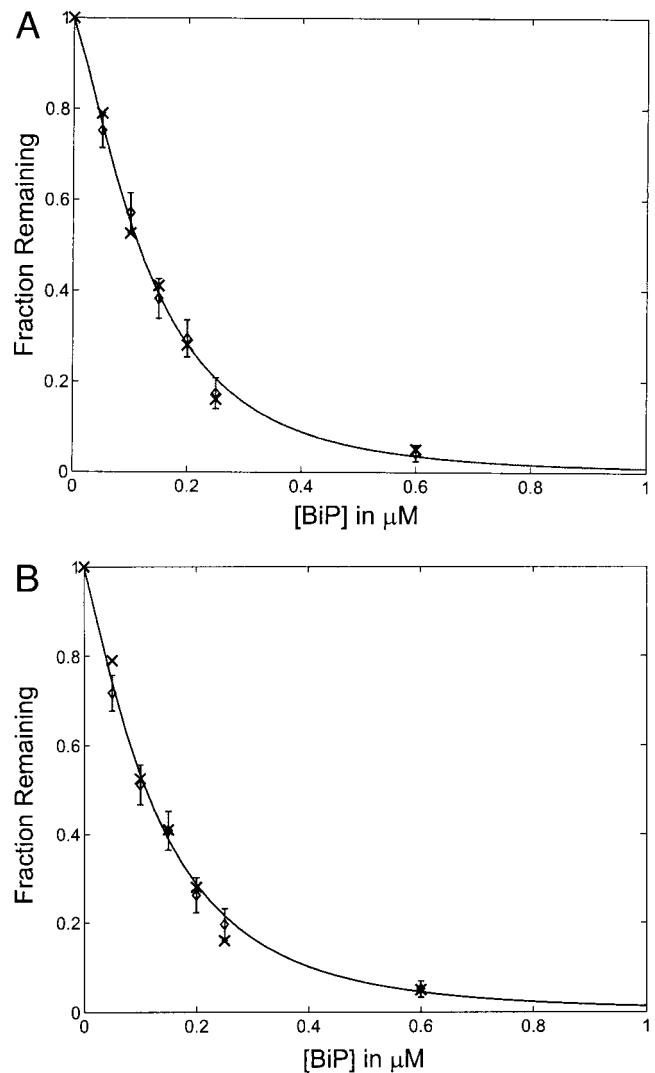
well. The PSM looks more exponential overall because once the first BiP molecule is bound, escape from free energy well is assisted by the power stroke. However, the BRM does produce a fairly good approximation.

Since the data have been globally fit, a likelihood-ratio test can be used to test whether the extra parameter in the PSM produces significantly better results. As discussed in Appendix B, the relevant quantity for this test is the ratio of the sum of the squared errors for the BRM to that of the PSM. This ratio is denoted as λ. Using the optimal parameters for both models, $\lambda = 1.18$. Nineteen data points have been fit (excluding the ones at $t = 0$). The two models are
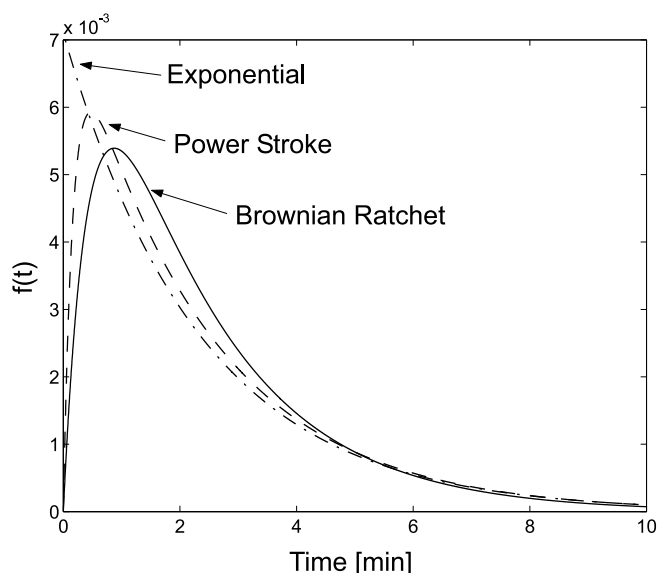
FIGURE 7 The first-passage time distributions for the translocation of prepro-α-factor. The solid and dashed curves are for the BRM and PSM, respectively. The dot-dashed curve is an exponential distribution characterized by $E[T] = 2.3$ min. The PSM captures the exponential character of the fraction-released data better than the BRM, because in this case once the first BiP molecule binds, release of the signal sequence is aided by a power stroke.

FIGURE 8 (A) A typical realization of the translocation process from a Monte Carlo simulation. The plot shows both the leading edge of a prepro-α-factor protein as the polypeptide moves through the channel and BiP binding and release events. The simulation lasts for 20 min. Once release occurs (at ~2.3 min), the position of the prepro-α-factor molecule is no longer monitored. (B) An expanded view of the time interval between 1.75 and 2.0 min illustrating that once the second BiP molecule binds, translocation proceeds rapidly.

nested, in that BRM represents the limiting case of the PSM with $F_{ps} \rightarrow 0$. Therefore, under the assumptions for the errors given in Appendix B, λ has an F distribution with 1 and 12 degrees of freedom. For the results to be significant at the 5% level, λ must be ≥ 4.75. Therefore, the BRM clearly cannot be ruled out given the data considered here. However, if instead of 19 data points there were an additional 48, and if the estimated variance of the errors remained the same, then λ would increase by a factor 67/19 and be significant at the 5% level.

MONTE CARLO SIMULATIONS

The procedure for parameter estimation used in the previous section was based on several mathematical assumptions. In particular, it was assumed that translocation proceeded instantaneously for segments of the polypeptide that did not include the signal sequence, and that all the translocation substrates were released with exactly the same number of BiP molecules bound to them. To verify the validity of these assumptions, I performed Monte Carlo simulations of the two models using the estimated parameter values. Only the case in which the signal sequence exits first was considered. The model used for the case in which the signal sequence exits last relies on the same mathematical assumptions. Therefore, the simulations also support these results. The Monte Carlo simulations are also used to investigate differences between specific and nonspecific BiP binding. In all
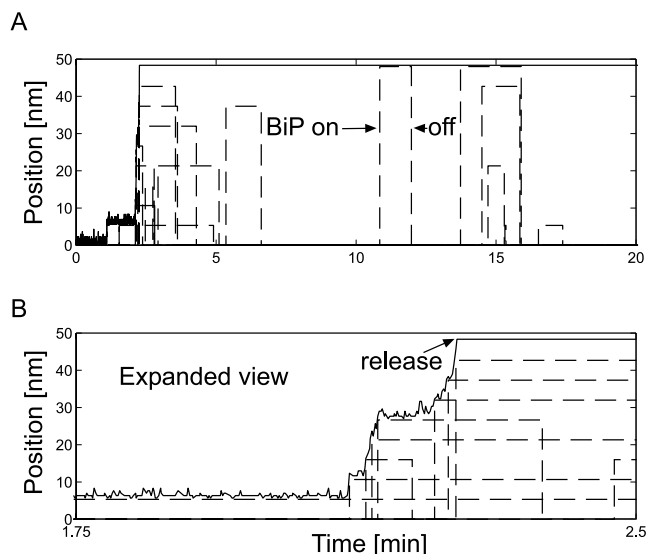
the results shown for the nonspecific binding case, I have assumed $k'_{on} = 0$. This assumption simplifies the numerical algorithm considerably, without significantly affecting the results.

Fig. 8 A shows a typical realization of the BRM when specific binding is assumed. Trajectories for the PSM and nonspecific binding cases are visually indistinguishable. The time series shows the leading edge as a prepro-α-factor protein passes through the channel. Once the polypeptide escapes (at close to 2.3 min), its position is no longer monitored. Fig. 8 B is an enlargement of the region between $t = 1.75$ min and $t = 2.5$ min. As can be seen, once the second BiP molecule binds, translocation proceeds rapidly. Also shown in these figures are BiP binding and dissociation events. The number of bound BiP molecules is monitored for the full 20-min interval. After the prepro-α-factor protein has been released, BiP molecules continue to bind at a rate $k'_{on}[BiP] < k_{on}[BiP]$.

To compare the simulations with experimental data an ensemble average was performed over 500 realizations of the process. Fig. 5, A and B show the results for the fraction-released data and fraction-released and free data. As can be seen, there is excellent agreement between Monte Carlo simulations and approximate methods, thus justifying the assumptions that once the signal sequence has escaped from the channel, translocation proceeds very rapidly, and that when prepro-α-factor is released it is densely packed with $N - 3$ BiP molecules. Also shown in these figures are
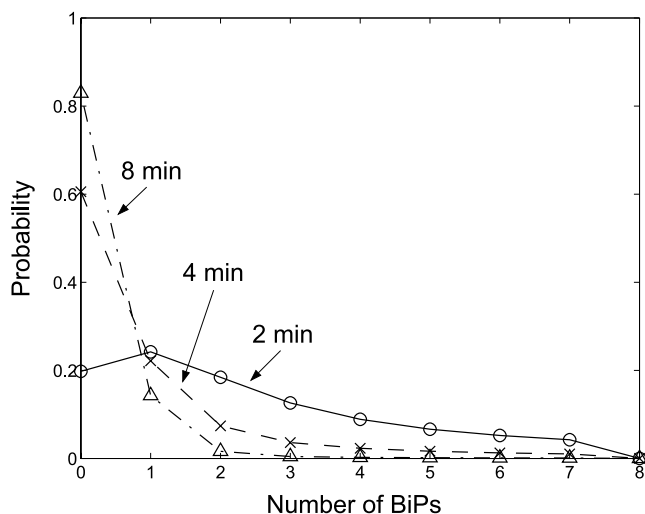
FIGURE 9 The probability distributions for the number of BiP molecules bound to a prepro-α-factor molecule at various times after release from the channel. The results shown here are for the BRM, but the PSM results look very similar. Two minutes after release multiple BiP molecules are bound to the translocation substrate, with the average close to 2.3. After 8 min most of the BiP molecules have been lost.
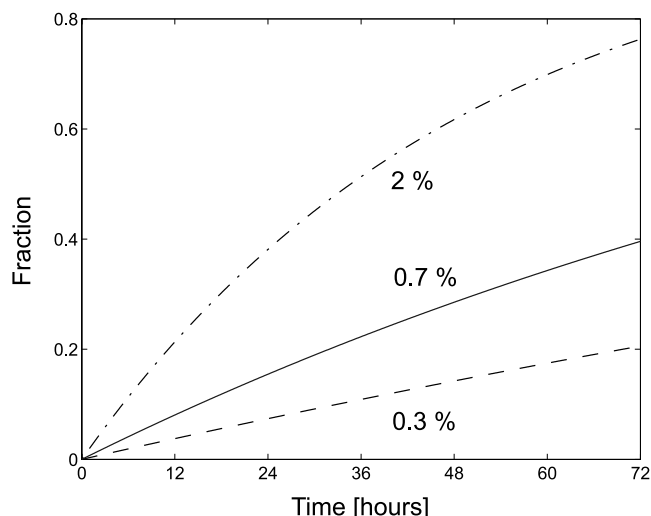

FIGURE 10 The fraction of prepro-α-factor released as a function of time in the absence of BiP. The experiments of Matlack et al. (1999) put an upper bound on the fraction released of 2% released after 1 h (*dot-dashed curve*). The BRM predicts this number to be $\sim$0.7% (*solid curve*) and the PSM predicts a value of 0.3% (*dashed curve*).

results for the fraction released for the case of nonspecific binding. These results have been offset by 0.3 for clarity. The only parameter that has been adjusted is k_{on}. For the BRM, k_{on} was reduced from 351 to 263 s^{-1} μM^{-1}, and for the PSM, k_{on} was reduced from 310 to 248 s^{-1} μM^{-1}. The nonspecific binding results are virtually identical to the specific binding results.

Finally, in Fig. 6, *A* and *B*, I present results for the fraction remaining after 10 min. The diamonds represent the nonspecific binding case. For clarity, I have not included the specific binding results. However, these points show equally good agreement with the simplified model as those presented for the fraction-released and fraction-released and free data. The good agreement between the curves and the Monte Carlo simulations further validates the approximate methods.

MATHEMATICAL CHARACTERIZATION

The simplified models can be used to compute the probability distributions for the number of BiP molecules bound to a released prepro-α-factor protein as a function of time. The results for the BRM are shown in Fig. 9. The results for the PSM are almost identical, and therefore are not shown. After 2 min, prepro-α-factor contains multiple BiP molecules, with an average number of $\sim$2.3 for both models. This is somewhat smaller than the reported value of 4 (Liebermeister et al., 2001). However, this discrepancy might be resolved if all the BiP molecules do not bind to prepro-α-factor with the same affinity. After 4 min the

average value is $\sim$1 BiP molecule per prepro-α-factor protein.

In Appendix C I show that for the BRM and PSM with nonspecific binding, the average distance between BiP molecules is

$$L_{Avg} = \sqrt{\frac{D}{k_{on}[BiP]}}. \qquad (10)$$

Therefore, both models predict that if BiP binds nonspecifically to prepro-α-factor, there should be an average distance of $\sim$1 nm between BiP molecules. If we assume that each BiP molecule is $\sim$4 nm in length, then prepro-α-factor should have up to 11 BiP molecules bound at release. This number is somewhat higher than the 6 to 7 molecules measured by Matlack et al. (1999). However, their measurements represent a lower bound.

One advantage of the PSM is that it can overcome stronger signal sequence/channel interactions than the BRM. Such strong interactions might be required for translocation selectivity. In the absence of BiP it was observed that <2% of the translocation substrates were released after 60 min (Liebermeister et al., 2001). We can use the estimated values of ΔG, D, and L_{BiP} to calculate the percent of prepro-α-factor released after 60 min. The results for the BRM are 1% and 0.7% for the cases in which the signal sequence leaves first and last, respectively. In both cases for the PSM, this number is close to 0.3%. Fig. 10 is a plot of the fraction of prepro-α-factor released in the absence of BiP. Experimental measurements of this type would place additional constraints on
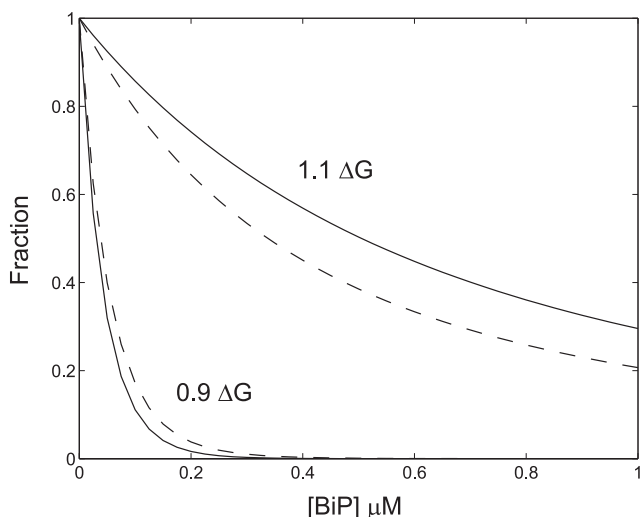
FIGURE 11   Theoretical predictions for the fraction of prepro-α-factor molecules still bound to the channel after 10 min as function of [BiP] for two different values of ΔG. To produce this figure the parameters estimated from the scenario in which the signal sequence leaves last have been used, in which case $F_{ps} = 3.8$ pN. A 10% change in the free energy produces differences in the fraction remaining that might be used to distinguish the models. The solid curves are for the BRM and the dashed curves are for the PSM.

the models and would be very useful in trying to determine the import mechanism.

The parameter on which the results are most sensitive is ΔG. However, if a power stroke of only 1.6 pN is involved in translocation, then even varying ΔG does not produce significant difference in the models' predictions. In the scenario in which the signal sequence leaves last a power stroke of 3.8 pN was found, in which case varying ΔG could provide a method for discriminating the two models. ΔG could be varied by mutating one or more amino acids of the signal sequence or by artificially applying an electric potential across the ER membrane. The effects of changing ΔG on the fraction remaining are shown in Fig. 11. With a 3.8 pN power stroke, a 10% change in ΔG produces significant differences in the models' predictions. Equation 7 can be used to find a relationship between ΔG and the interaction free energy ΔG_m of the modified system

$$\frac{E[T_{nBiP}]}{E[T_m]} = \frac{\Delta G_m}{\Delta G} \exp\left(\frac{\Delta G - \Delta G_m}{k_B T}\right) \qquad (11)$$

where $E[T_m]$ is the average time for release of prepro-α-factor from the channel in the absence of BiP for the modified system. Both mean values on the left-hand side of the above expression can be determined from data for the fraction released in the absence of BiP.

Next, the fraction-released calculations are repeated at different BiP concentrations. The results for the case in
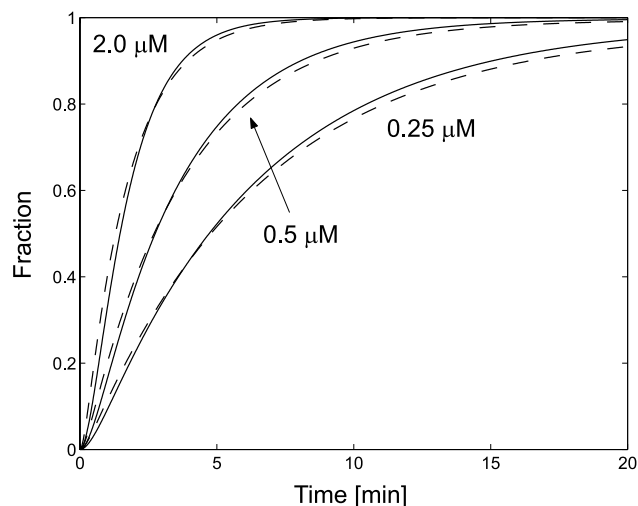

FIGURE 12   Theoretical predictions for the fraction of prepro-α-factor molecules released from the channel as a function of time for various different BiP concentrations. The solid curves are for the BRM and the dashed curves are for the PSM.

which the signal sequence leaves first are shown in Fig. 12. The two models show only slight differences, and these experiments probably cannot be used to distinguish them. However, these are predictions that can be used to validate the assumptions common to both models. Also, if these data become available, they can be used in a global fit to better estimate parameter values. I have also repeated the calculations for the fraction-released and free at different BiP concentrations. Again, the two models produced only minor difference, but such data would also be useful for testing the models and estimating parameters.
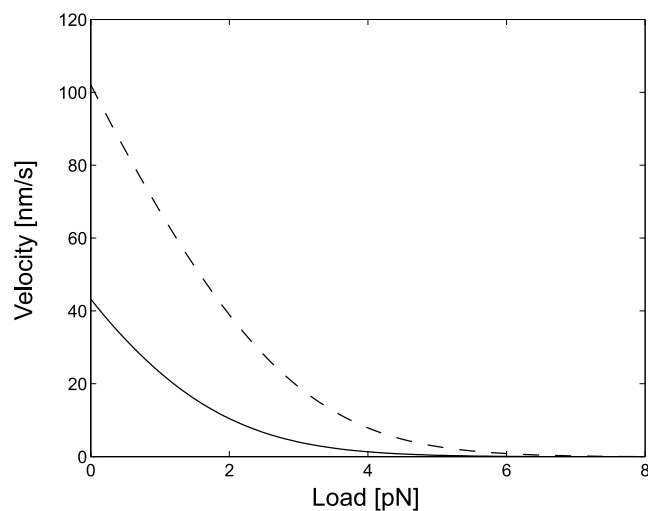

FIGURE 13   The predicted load-velocity plots for both models at 1 μM BiP. The solid curve is for the BRM and the dashed curve is for the PSM. The PSM produces a significantly larger no-load velocity than the BRM.

Finally, the steady-state properties of the system are considered. I begin by computing load-velocity plots for both models. This has been a useful method for characterizing the mechanical properties of other motor proteins. However, such measurements for translocation systems have not yet been done. Fig. 13 shows the average velocity as a function of applied load at 1 μM BiP. In the figure I have used the parameter values determined when the signal sequence exits first. Not surprisingly, the qualitative features of the two curves are similar. However, the average no-load velocities of the PSM (close to 100 nm/s) is considerably larger than that of the BRM (close to 40 nm/s).

Finally, the average velocity as a function of BiP concentration is considered. The maximum velocity of the BRM with either specific or nonspecific binding is

$$\nu_{max} = \frac{2D}{L_{BiP}} \tag{12}$$

Using the parameter values for the first-out scenario, the maximum velocity is 53.3 nm/s. The maximum velocity of the PSM with either type of binding is (Elston, 2000b)

$$\nu_{max} = \frac{D}{L_{BiP}} \left[\frac{\left(\frac{F_{ps}L_{BiP}}{k_BT}\right)^2}{\exp\left(-\frac{F_{ps}L_{BiP}}{k_BT}\right) + \frac{F_{ps}L_{BiP}}{k_BT} - 1} \right] \tag{13}$$

which reduces to Eq. 12 in the limit $F_{ps} \to 0$. The maximum velocity of the PSM is 123.8 nm/s.

In earlier work, Elston (2000b) showed that if the chemical kinetics was much faster than the motion of the trans-

locating polypeptide (i.e., k_{on} and $k_{off} \gg D/L_{BiP}^2$), then both models show Michaelis-Menten kinetics in the average velocity as a function of [BiP]. This was assumed to be the appropriate limit, because the strong interaction between the signal sequence and the channel complex was not taken into account. However, including this effect reveals that the fast kinetics approximation is not the relevant limit for the process. If the assumption is made that $k_{off} = 0$, it is possible to work out expressions for the average velocity for both models and both types of binding. For the BRM with specific binding the average velocity is (Elston, 2000b)

$$\nu = \frac{2D}{L_{BiP}} \frac{\sqrt{[BiP]}}{\frac{2}{\sqrt{\alpha}} + \sqrt{[BiP]}} \tag{14}$$

where $\alpha = L_{BiP}^2 k_{on}/D$. The above result is valid when $\exp[(4\ \alpha)^{1/2}] \gg 0$ and $k_{on}[BiP] \gg k_{off}$. For nonspecific binding, Liebermeister et al. (2001) have shown that the average velocity of the BRM is

$$\nu = \frac{2D}{L_{BiP}} \left[\frac{\sqrt{\alpha[BiP]} + \alpha[BiP]}{2(1 + \sqrt{\alpha[BiP]}) + \alpha[BiP]} \right] \tag{15}$$

In Appendix C I extend Liebermeister et al.'s calculation to include a power stroke. The result is

$$\nu = \frac{D}{L_{BiP}} \{[\omega^2 e^\omega(\sqrt{\alpha[BiP]} + \alpha[BiP])\}$$
$$\div \{\alpha[BiP][\omega e^\omega - (e^\omega - 1)]$$
$$+ \omega[e^\omega(\omega + \sqrt{\alpha[BiP]}) - \sqrt{\alpha[BiP]}]\} \tag{16}$$

where $\omega = F_{ps}L_{BiP}/k_BT$. Equation 16 reduces to Eq. 15 in the limit $F_{ps} \to 0$. The result for the specific binding case is considerably more complicated and not enlightening, therefore, I do not present it here. Fig. 14 summarizes the results for the average velocity as a function of [BiP]. The two different types of binding place upper (nonspecific) and lower (specific) bounds on the velocity for the two models.

DISCUSSION

Earlier theoretical results for post-translational translocation were derived from the assumption that the chemical kinetics of BiP binding was fast as compared to the time scale set by thermal diffusion (L_{BiP}^2/D) (Elston, 2000b; Simon et al., 1992). However, these investigations did not consider the strong interaction between the signal sequence and channel complex. When this effect is taken into account, the fast kinetics assumption is no longer valid. However, the effective diffusion coefficient D is still over two orders of magnitude smaller than what would be expected for a protein diffusing through a large
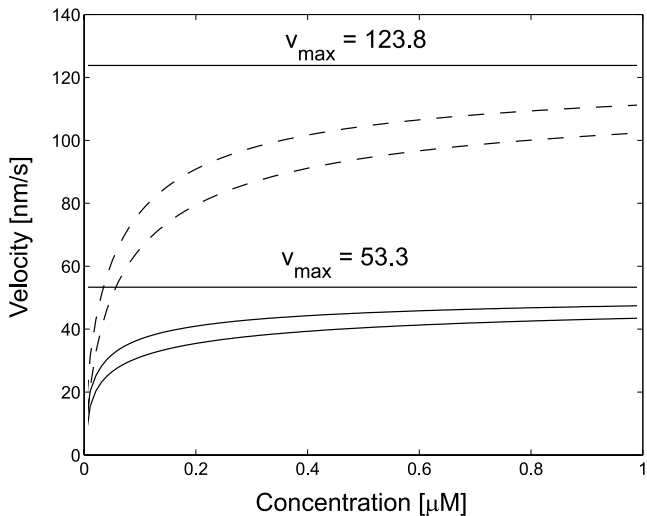

FIGURE 14 The average velocity as a function of [BiP] for both models and both types of BiP binding. The solid curves are for the BRM and the dashed curves for the PSM. The case of nonspecific BiP binding places an upper bound on the velocity and the case of specific binding is a lower bound.

channel. This indicates that prepro-α-factor does interact with the walls of the channel during translocation. The nature of this interaction (entropic, hydrophobic, electrostatic, etc.) is not clear. A similar effect was found in experiments that measured the kinetics of nonelectrolytic polymers partitioning into ion channels (Bezrukov et al., 1996). In this study the reduced diffusion coefficient was attributed to hydrophobic interactions between the polymer and the channel walls.

In a recent paper, Liebermeister et al. (2001) used a Brownian ratchet model to fit translocation data. It is informative to compare and contrast the modeling techniques used by those authors and the ones presented here. In their analysis, the motion of the translocating peptide is modeled using a Markov chain. That is, the translocation substrate moves in discrete steps characterized by a transition rate s. I have taken the position of the translocation substrate to be continuous and modeled polypeptide-channel interactions through an effective diffusion coefficient D. Therefore, my method represents the limiting case of the Liebermeister model in which the number of steps taken by the translocating polypeptide becomes infinite. Liebermeister et al. assumed 10 steps were required to move prepro-α-factor through the channel, and each step represented a BiP binding site. The best fit to the data was achieved when $s = 0.2$ s^{-1}. This should be compared with the value $D/L_{BiP}^2 = 4.4$ s^{-1} and 5.4 s^{-1} for the BRM and PSM, respectively. The reason for the considerably slower rate in the Liebermeister model is that a value of $\Delta G = 20$ kJ/mol was used, which is considerably smaller than the values found here ($\sim$50 kJ/mol). Liebermeister et al. assumed that ΔG represented the free energy need to unfold prepro-α-factor as it passed through the channel, and spread it evenly over the first four steps. Since this does not produce a single rate-limiting step, the exponential character of the fraction-released data was not captured. In our approach ΔG represents the free energy arising from the interaction between the signal sequence and the channel. Therefore, the length of this interaction was limited to the first two binding sites, which roughly corresponds to the length of the signal sequence. This allowed the exponential character of the fraction-released data to be reproduced, and the rate-limiting step was found to be the binding of the first BiP molecule. Limiting the free energy barrier to the first two sites required using larger values of ΔG and D. It also required using significantly higher J-activated association rates, roughly 300 μM^{-1} s^{-1}, as compared to 1 μM^{-1} s^{-1} in the Liebermeister model. These rates are also considerably faster than those measured for DnaK and peptides (0.45 μM^{-1} s^{-1}) (Schmid et al., 1994). However, these measurements were not done for translocating proteins in which the J-domain and peptide are held in close apposition by the channel. Therefore, for either of the models considered here to be valid, having

prepro-α-factor threaded through the channel must significantly increase k_{on}.

The value of k_{off} determined by Liebermeister et al. was 0.017 s^{-1}, which compares favorably to the values of $\sim$0.027 s^{-1} found here. The slight discrepancy may be attributable to the fact that Liebermeister et al. did not allow BiP to bind to prepro-α-factor after its release from the channel (i.e., $k'_{on} = 0$). Including a nonzero k'_{on} produced a better fit to the fraction-released and free data and allowed a dissociation constant for BiP binding to be computed. The values of K_d, 62 μM and 66 μM for the BRM and PSM, respectively, are in reasonable agreement with the values measured by Misselwitz et al. (1998). For all the data considered here, the continuous models produce a better fit to the data. However, before the models can be accepted, the estimated parameter values must be validated through independent experimental measurements.

Unfortunately, the theoretical analysis did not produce a clear-cut method for distinguishing the BRM and PSM. However, it did reveal the significance of the strong interaction between the signal sequence and channel in the translocation process. The parameter ΔG characterizes the strength of this interaction and is the parameter on which the results are most sensitive. This is reasonable, because a power stroke provides a considerable advantage when the translocation substrate must escape over a free energy barrier. Presumably, ΔG can be changed by mutating one or more residues in the signal sequence or by applying an electrostatic potential across the ER membrane. Experimentally determining ΔG might be accomplished by measuring the fraction of prepro-α-factor released in the absence of BiP as a function of temperature. This should reveal Arrhenius dependence of the mean release time on ΔG.

A global fit to the data was performed. Therefore, if the models are valid, they should be able to reproduce any new experimental data with minimal parameter adjustment. For the BRM, six parameters, k_{off}, k'_{on}, N, ΔG, D, and k_{on} were estimated. The PSM has one additional parameter to fit, F_{ps}. As shown through a likelihood-ratio test, the limited data considered here are not sufficient to eliminate the BRM as an import mechanism. I believe as more data become available, statistical inference will become an even more valuable tool for discriminating theoretical models of post-translational translocation.

APPENDIX A: NUMERICAL METHODS

Modeling the fraction-released and free data

Let the random variable $M(t)$ denote the number of BiP molecules bound to a free prepro-α-factor protein with N binding sites. At the time of release from the channel, there are exactly l BiP molecules bound to the polypep-

tide. The probabilities $p_m(t) = \text{Pr}[M(t) = m]$ are described by the following set of equations:

$$\frac{dp_N}{dt} = -Nk_{off}p_N + k'_{on}[\text{BiP}]p_{N-1} \tag{17}$$

$$\frac{dp_{N-1}}{dt} = -[(N-1)k_{off} + k'_{on}[\text{BiP}]]p_{N-1}$$
$$+ Nk_{off}p_N + 2k'_{on}[\text{BiP}]p_{N-2} \tag{18}$$
$$\vdots$$

$$\frac{dp_\ell}{dt} = -[lk_{off} + (N-l)k'_{on}[\text{BiP}]]p_\ell$$
$$+ (l+1)k_{off}p_{\ell+1}$$
$$+ (N-l+1)k'_{on}[\text{BiP}]p_{\ell-1} + j_{out}(t) \tag{19}$$
$$\vdots$$

$$\mathbf{M} = \begin{pmatrix} -(k_{on}[\text{BiP}] + k'_{on}[\text{BiP}]) & k_{off} & k_{off} & 0 \\ k'_{on}[\text{BiP}] & -(k_{on}[\text{BiP}] + k_{off}) & 0 & k_{off} \\ k_{on}[\text{BiP}] & 0 & -(k'_{on}[\text{BiP}] + k_{off}) & k_{off} \\ 0 & k_{on}[\text{BiP}] & k'_{on}[\text{BiP}] & -2k_{off} \end{pmatrix} \tag{25}$$

$$\frac{dp_1}{dt} = -[k_{off} + (N-1))k'_{on}[\text{BiP}]]p_1$$
$$+ 2k_{off}p_2 + Nk'_{on}[\text{BiP}]p_0 \tag{20}$$

$$\frac{dp_0}{dt} = -Nk'_{on}[\text{BiP}]p_0 + k_{off}p_1 \tag{21}$$

where $j_{out}(t)$ in Eq. 19 is the flux of prepro-α-factor out of the channel. If we assume that prepro-α-factor is released from the channel at an exponential rate k_{out}, then $j_{out} = k_{out} \exp(-k_{out}t)$. To globally fit all the data, j_{out} is computed numerically by solving the appropriate diffusion equation (see next section). The initial conditions are $p_m(0) = 0$ for $m = 0, \ldots, N$. The Crank-Nicolson algorithm was used to numerically integrate the above set of ordinary differential equations and $p_0(t)$ was fit to the fraction-released and free data.

Modeling the fraction-released data and fraction-remaining data

For the case of specific binding, the state of the system is described by the random variables $X(t)$; the distance between the channel and the rear edge of the first completely translocated binding site, C; the number of trans-located binding sites, and the C-dimensional vector $\mathbf{S}$, whose elements correspond to the state of the translocated binding sites. The S_i element of $\mathbf{S}$ is equal to 1 if the ith site is occupied, and 0 otherwise. Therefore, with C sites translocated, there are 2^C chemical states for the translocation

substrate. The diffusion equation and boundary conditions for this process can be found in Elston (2000b). As an example, consider the case of $C = 2$. Let $\rho_{ij}(x, 2, t)dx = \text{Pr}[S_1 = i, S_2 = j, x \le X(t) \le x + dx, C(t) = 2]$. The diffusion equation for $\boldsymbol{\rho} = (\rho_{01}, \rho_{01}, \rho_{01}, \rho_{01})$ is

$$\frac{\partial \boldsymbol{\rho}}{\partial t} = \mathbf{L}\boldsymbol{\rho} + \mathbf{M}\boldsymbol{\rho} \tag{22}$$

The elements of the diagonal matrix operator $\mathbf{L}$ are

$$L_i = D\left(\frac{1}{k_B T}\frac{\partial}{\partial x}\left(\frac{\partial G(x)}{\partial x}\right) + \frac{\partial^2}{\partial x^2}\right) \quad \text{for} \quad i = 1 \text{ and } 3 \tag{23}$$

$$L_i = D\left(\frac{1}{k_B T}\frac{\partial}{\partial x}\left(\frac{\partial G(x)}{\partial x}\right) - \frac{F_{ps}}{k_B T}\frac{\partial}{\partial x} + \frac{\partial^2}{\partial x^2}\right)$$
$$\text{for} \quad i = 2 \text{ and } 4 \tag{24}$$

where $G(x)$ is the free energy as shown in Fig. 4 A. The transition matrix $\mathbf{M}$ is given by

Equation 22 is solved using the numerical algorithm described by Mogilner et al. (2001). For the case in which the signal sequence leaves first the spatial interval is $(0, 3 L_{BiP})$ and for the case in which the signal sequence leaves last it is $(0, 2 L_{BiP})$. To model release from the channel, an absorbing barrier is placed at the right end of the interval; $x = 3 L_{BiP}$ or $2 L_{BiP}$. The numerically computed flux at the absorbing boundary is used in Eq. 19. A reflecting barrier is placed at the bottom of the free energy well at $x = 0$. This simplifies the numerical algorithm, but does not significantly affect the results because in the presence of BiP, back-diffusion out of the channel is very unlikely.

For the steady-state results only the first two binding sites within the lumen are taken into account. The third site is assumed to be empty. This assumption does not affect the results because at high BiP concentrations prepro-α-factor has a very low probability of back-diffusing two full sites, and at low BiP levels this site is likely to be empty.

APPENDIX B: THE LIKELIHOOD-RATIO TEST

The experimental data points can be written as the set of ordered pairs (x_i, y_i), where x_i is the value of a controllable experimental parameter and y_i is the measured result at x_i. Let $z_i(x_i, \boldsymbol{\theta})$ be the model output, where the vector $\boldsymbol{\theta}$ contains the model parameters. Then

$$y_i = z_i(x_i, \boldsymbol{\theta}) + \epsilon_i \tag{26}$$

where ϵ_i is the error between the experimental result and the model's predicted value. The source of this error might be imprecision in the experimental measurements, mathematical approximations, or invalid

model assumptions. If we assume the errors are statistically independent and normally distributed with mean zero and identical variances σ^2, the likelihood function is

$$L(\boldsymbol{\theta}, \sigma^2) = \prod_{i=1}^{n} \frac{1}{\sqrt{2\pi\sigma^2}} \exp\left(-\frac{1}{2\sigma^2}[y_i - z_i(x_i, \boldsymbol{\theta})]^2\right) \quad (27)$$

where n is the number of data points. Maximizing L with respect to σ and $\boldsymbol{\theta}$ provides the best estimates for these parameters given the assumption of independence and normality of the errors. The constraint on the variance, found by equating the derivative of L with respect to σ^2 equal to zero, is

$$\sigma^2 = \frac{1}{n} \sum_{i=1}^{n} [y_i - z_i(x_i, \theta)]^2 \quad (28)$$

from which we find

$$\max L = \max\left[\left(\frac{n}{2\pi\sum_{i=1}^{n}[y_i - z_i(x_i, \theta)]^2}\right)^{n/2} \exp\left(-\frac{n}{2}\right)\right] \quad (29)$$

Therefore, for this case maximizing L is equivalent to minimizing the sum of the squared errors (least squares).

Let L_P and L_B be the likelihood functions for the PSM and BRM, respectively. Then

$$\frac{\max L_p}{\max L_B} = \left(\frac{\min \sum_{i=1}^{n} [y_i - z_i^B(x_i, \boldsymbol{\theta})]^2}{\min \sum_{i=1}^{n} [y_i - z_i^P(x_i, \boldsymbol{\theta})]^2}\right)^{n/2} \geq K \quad (30)$$

where z_i^P and z_i^B are for the PSM and BRM, respectively, and K is the value that produces a 5% significance level for the ratio of the likelihood functions. The above inequality can be rewritten as

$$\lambda = \left(\frac{\min \sum_{i=1}^{n} [y_i - z_i^B(x_i, \theta)]^2}{\min \sum_{i=1}^{n} [y_i - z_i^P i(x_i, \theta)]^2}\right) \geq K^{2/n} = k \quad (31)$$

where λ is the ratio of the estimated variances of the two models. The standard result is that as the number of data points becomes large, $2 \ln(\lambda)$ is distributed as chi-square with one degree of freedom. However, given the limited amount of data, I prefer to be conservative and perform an F-test for the ratio of two variances. In this case, the degrees of freedom are 1 (7 parameters − 6 parameters = 1) and 12 (19 data points − 7 parameters = 12). Then, $k = 4.75$ is the 5% significance level.

APPENDIX C: NONSPECIFIC BINDING

The average distance between BiP molecules

To calculate the average velocity for the case of nonspecific binding, it is necessary to know the average spacing between BiP molecules bound to a prepro-α-factor molecule. It turns out this spacing is independent of whether translocation is driven by a BRM or PSM. The average spacing can be calculated as follows. Let $X(t)$ denote the distance between the channel and the first bound BiP. A second BiP can bind only when $X(t) \geq L_{BiP}$. Therefore, we do not need to consider values of $X(t) < L_{BiP}$. Let $Y(t) = X(t) - L_{BiP}$. The distribution for $Y(t)$ given $Y(0) = 0$ and not allowing $Y(t) < 0$ is

$$\rho(y, t) = \frac{2}{\sqrt{4\pi Dt}} \exp\left(-\frac{y^2}{4Dt}\right) \quad (32)$$

From which we find $E[Y(t)] = \mathrm{Sqrt}(4Dt/\pi)$. BiP binds at an average rate $k = k_{on}[BiP]$; therefore, the time in the expected value of $Y(t)$ is also a random variable. To compute the average spacing, we average with respect to this time

$$L_{avg} = \int_0^\infty E[Y(t)]ke^{-kt}dt = \sqrt{\frac{D}{k}} = \sqrt{\frac{D}{k_{on}[BiP]}} \quad (33)$$

The above result has been verified numerically.

The average velocity

To compute the average velocity I follow the elegant analysis of Liebermeister et al. (2001). In this method, the translocation substrate is initially assumed to move in discrete steps. The velocity is then computed in the limit that the step size goes to zero. The translocation substrate must move through at least K steps before the next BiP molecule can bind. Let $X(t) = \Delta x M(t)$, where $M(t) \in (0,1,2, \ldots)$ and $\Delta x = L_{BiP}/K$, denote the position of the rear edge of the BiP molecule nearest the channel, and let $p_m(t) = \Pr[M(t) = m]$. The master equation for this process is

$$\frac{dp_0}{dt} = -\gamma\kappa p_0 + \frac{\gamma}{\kappa} p_1 + k \sum_{i=K}^{\infty} p_i \quad (34)$$

$$\frac{dp_m}{dt} = -\left(\gamma\kappa + \frac{\gamma}{\kappa}\right)p_m + \gamma\kappa p_{m-1} + \frac{\gamma}{\kappa} p_{m+1}$$
$$\text{for} \quad m = 1, \ldots, K-1 \quad (35)$$

$$\frac{dp_K}{dt} = -\left(\gamma + \frac{\gamma}{\kappa} + k\right)p_\kappa + \gamma\kappa p_{\kappa-1} + \gamma p_{\kappa+1} \quad (36)$$

$$\frac{dp_m}{dt} = -(2\gamma + k)p_m + \gamma p_{m-1} + \gamma p_{m+1} \quad \text{for } m > \kappa \quad (37)$$

where $\gamma = D/\Delta x^2$, $\kappa = \exp(F_{ps} \Delta x/k_B T)$, and $k = k_{on}[BiP]$. The same technique as described by Liebermeister et al. (2001) is used to find the steady-state solutions to Eqs. 34–37. The flux is given by

$$J = \gamma\kappa p_0^s - \frac{\gamma}{\kappa} p_1^s \quad (38)$$

From which the average velocity ν is found

$$\nu = (L_{BiP} + L_{avg})J \quad (39)$$

Finally, when the limit $K \to \infty$ is taken, Eq. 16 is obtained.

REFERENCES

Bezrukov, S., I. Vodyanoy, R. Brutyan, and J. Kasianowicz. 1996. Dynamics and free energy of polymers partitioning into a nanoscale pore. *Macromolecules.* 29:8517–8522.

Brodsky, J., and R. Schekman. 1993. A Sec63-BiP complex from yeast is required for protein translocation in a reconstituted proteoliposome. *J. Cell Biol.* 123:1355–1363.

Chauwin, J. F., G. Oster, and B. S. Glick. 1998. Strong precursor-interactions constrain models for mitochondrial import. *Biophys. J.* 74:1732–1743.

Corsi, A., and R. Schekman. 1997. The lumenal domain of Sec63p stimulates the ATPase activity of BiP and mediates BiP recruitment to the translocon in *Saccharomyces cerevisiae. J. Cell Biol.* 137:1483–1493.

Deshaies, R., S. Sanders, D. Feldheim, and R. Schekman. 1991. Assembly of yeast Sec proteins involved in translocation into the endoplasmic reticulum into a membrane-bound multisubunit complex. *Nature.* 349:806–808.

Elston, T. 2000a. A macroscopic description of biomolecular transport. *J. Math. Biol.* 41:189–206.

Elston, T. 2000b. Models of post-translational protein translocation. *Biophys. J.* 79:2235–2251.

Glick, B. 1995. Can Hsp70 proteins act as force-generating motors? *Cell.* 80:11–14.

Gorlich, D., and T. Rapoport. 1993. Protein translocation into proteoliposomes reconstituted from purified components of the endoplasmic reticulum membrane. *Cell.* 75:615–630.

Liebermeister, W., T. Rapoport, and R. Heinrich. 2001. Ratcheting in posttranslational protein translocation: a mathematical model. *J. Mol. Biol.* 305:643–656.

Lubensky, D., and D. Nelson. 1999. Driven polymer translocation through a narrow pore. *Biophys. J.* 77:1824–1838.

Lyman, S., and R. Schekman. 1995. Interaction between BiP and Sec63p is required for the completion of protein translocation into the ER of *Saccharomyces cerevisiae. J. Cell Biol.* 131:1163–1171.

Matlack, K., B. Misselwitz, K. Plath, and T. Rapoport. 1999. BiP acts as a molecular ratchet during posttranslational transport of prepro-α factor across the ER membrane. *Cell.* 97:553–564.

Matlack, K., K. Plath, B. Misselwitz, and T. Rapoport. 1997. Protein transport by purified yeast complex and Kar2p without membranes. *Science.* 277:938–941.

Misselwitz, B., O. Staeck, and T. Rapoport. 1998. J proteins catalytically activate Hsp70 molecules to trap a wide range of peptide sequences. *Mol. Cell.* 2:593–603.

Mogilner, A., T. Elston, H. Wang, and G. Oster. 2001. Molecular Motors: Theory. *In* Keizer's Computational Cell Biology. C. Fall, E. Marland, J. Tyson, and J. Wagner, editors. Springer, New York.

Muthukumar, M. 1999. Polymer translocation through a hole. *J. Chem. Phys.* 111:10371–10374.

Muthukumar, M. 2001. Translocation of a confined polymer through a hole. *Phys. Rev. Lett.* 86:3188–3191.

Panzer, S., L. Dreier, E. Hartmann, S. Kostka, and T. Rapoport. 1995. Posttranslational protein transport in yeast reconstituted with a purified complex of Sec Proteins and Kar2p. *Cell.* 81:561–570.

Park, P., and W. Sung. 1996. Polymer translocation through a membrane pore. *Phys. Rev. Lett.* 77:783–786.

Plath, K., W. Mothes, B. Wilkinson, C. Stirling, and T. Rapoport. 1998. Signal sequence recognition in posttranslational protein transport across the yeast ER membrane. *Cell.* 94:795–807.

Sanders, S., K. Whitfield, J. Vogel, and R. Schekman. 1992. Sec61p and BiP directly facilitate polypeptide translocation into the ER. *Cell.* 69:353–365.

Schmid, D., A. Baici, H. Gehring, and P. Christen. 1994. Kinetics of molecular chaperone action. *Science.* 263:971–973.

Schneider, H. J., J. Berthold, M. Bauer, K. Dietmeier, B. Guiard, M. Brunner, and W. Neupert. 1994. Mitochondrial Hsp70/MIM44 complex facilitates protein import. *Nature.* 371:768–774.

Simon, S., and G. Blobel. 1991. A protein-conducting channel in the endoplasmic reticulum. *Cell.* 65:371–380.

Simon, M. S., C. S. Peskin, and G. Oster. 1992. What drives the translocation of proteins? *Proc. Natl. Acad. Sci. USA.* 89:3770–3774.

Vogel, J., L. Mirsa, and M. Rose. 1990. Loss of BiP/GRP78 function blocks translocation of secretory proteins in yeast. *J. Cell Biol.* 110:1885–1895.